Field Emission Scanning Electron Microscopy for Structural Characterization of 3D Gold Nanoparticle Superlattices

Hiroshi Yao[*], and **Keisaku Kimura**

Graduate School of Material Science, University of Hyogo, 3-2-1 Koto, Kamigori-cho, Ako-gun, Hyogo, 678-1297, Japan

We prepared micrometer-sized three-dimensional (3D) superlattices of gold nanoparticles protected by *N*-acetylglutathione (NAG). The nanoparticles were self-assembled at an air/water interface under a highly acidic condition. Morphological studies revealed that the superlattices formed fivefold symmetric structures such as decahedron and icosahedron, which were probably developed by multiple twinning. High-resolution surface images of the superlattices obtained by FE-SEM showed excellent ordered arrangements of nanoparticles with either close-packed or non-close-packed structures.

Keywords nanoparticle superlattices; field emission scanning electron microscope (FE-SEM); fivefold symmetry; monolayer-protected gold nanoparticles

1. Introduction

The size range in nanoscience is typically from hundreds of nanometers down to the atomic level (approximately 0.2 nm), in which the materials (nanomaterials) can have different or enhanced chemical/physical properties compared to the same ones at a larger bulk size [1–5]. Two main origins for these features are an increased relative surface area and the dominance of quantum effects. An increase in specific surface area will result in a corresponding increase in chemical reactivity, making some nanomaterials useful as catalysts to improve the efficiency of fuel cells or batteries. As the size of matter is reduced to tens of nanometers or less, quantum effects can begin to play a role, and change the material's optical, magnetic or electrical properties significantly [3]. For example, gold nanoparticles can appear blue, red, or yellow in color as a function of their size. For intended applications using nanoparticles, the crucial challenge has been to make all nanoparticles the same size [2].

On the other hand, another emphasis has been placed on the shape control of nanomaterials because in many cases it allows one to fine tune the properties with a greater versatility than can be achieved otherwise [6–8]. In face-centered cubic (fcc) metal particles, for example, the crystallographic {111} and {100} surfaces are different not only in the surface atom densities but also in surface energies, so that single-crystalline silver or gold nanoparticles with sizes smaller than ~10 nm show intriguing particle shapes such as truncated octahedra or cuboctahedra [9–10]. In addition, twinned metal particles are found [9–10]. Twinning is the result of two subgrains sharing a common crystallographic plane, and thus, multiple twinning on alternate coplanar planes produces cyclic twinned polyhedra (decahedra and icosahedra) where the twinned tetrahedral subunits are arranged around fivefold axes [11].

Furthermore, construction of superstructures (ordered assemblies or superlattices) of nanomaterials is of recent key interest not only in future electronics applications but also in fundamental nanoscience [12–17]. Metal (gold and/or silver) nanoparticles are ideal "building blocks" for two- (2D) and three-dimensional (3D) superlattice structures. Preparation of ordered assemblies often requires surface passivation of the building blocks to protect against modifications of their properties by their environment, as well as to inhibit sintering. The organic surface protection of nanoparticles enables to self-assemble into their superlattices, so that controlling the chemical functionality of the organic monolayer allows the collective properties of the nanoparticle superlattices to be engineered [12].

[*] Corresponding author: e-mail: yao@sci.u-hyogo.ac.jp, Phone: +81 791-58-0160

Unlike the most successful approaches that utilize hydrophobic alkanethiols as a surface modifier in gold nanoparticles [13–17], we have developed the syntheses of carboxylate-protected water-soluble gold nanoparticles [18–20]. Application of such hydrophilic nanoparticles is one of the new fields for the construction of 3D superlattices not by weak van der Waals interaction but by strong hydrogen-bonding and/or electrostatic interactions [19,20]. Indeed, we have succeeded in preparing single-crystalline 3D superlattices consisting of mercaptosuccinic acid-protected gold nanoparticles. The superlattices form at an air/water interface under highly acidic conditions (pH < 2), and they are connected through hydrogen bonds among the surface carboxylic acids [21–24].

In the present study, we report construction of 3D superlattices consisting of *N*-acetylglutathione (NAG)-protected gold nanoparticles and their structural characterization using high-resolution electron microscopy. Glutathione (γ-glu-cys-gly) is one of the favorable surface protecting agents that contain both carboxyl and amino groups [18], so that it can be zwitterions under near-neutral pH conditions. The *N*-acetylation of the amino group in glutathione inhibits to produce the zwitterion, and the strategy for preparing nanoparticle superlattices via hydrogen-bonding among carboxylic acid molecules can be applied. During the superlattice characterizations, we found that fivefold symmetric (pentagonal, decahedral, and icosahedral) superstructures could be built from the NAG-protected gold nanoparticles.

2. High-resolution electron microscopy: FE-SEM

Nanotechnology has strongly driven the development of recent electron microscopy, with demands not only for increasing resolution but also for more information from the sample. Electron microscopes use a beam of highly energetic electrons to probe objects on a very fine scale [9, 25]. In standard electron microscopes, electrons are mostly generated by “heating” a tungsten filament (electron gun). They are also produced by a crystal of LaB_6. The use of LaB_6 results in a higher electron density in the beam and a better resolution than that with the conventional device. In a field emission (FE) electron microscope, on the other hand, no heating but a so-called "cold" source is employed. Field emission is the emission of electrons from the surface of a conductor caused by a strong electric field. An extremely thin and sharp tungsten needle (tip diameter 10–100 nm) works as a cathode. The FE source reasonably combines with scanning electron microscopes (SEMs) whose development has been supported by advances in secondary electron detector technology. The acceleration voltage between cathode and anode is commonly in the order of magnitude of 0.5 to 30 kV, and the apparatus requires an extreme vacuum ($\sim 10^{-6}$ Pa) in the column of the microscope. Because the electron beam produced by the FE source is about 1000 times smaller than that in a standard microscope with a thermal electron gun, the image quality will be markedly improved; for example, resolution is on the order of ~2 nm at 1 keV and ~1 nm at 15 keV. Therefore, the FE scanning electron microscope (FE-SEM) is a very useful tool for high-resolution surface imaging in the fields of nanomaterials science.

Additionally, we can conduct SEM-based scanning transmission electron microscope (STEM) imaging, that is, STEM can be carried out in an SEM by adding different detectors [26]. A fine, highly focused beam of electrons is scanned over a thin specimen, and the electrons that pass through the thin sample are collected on a detector placed beneath the sample, yielding the desired bright-field images. The bright field image in the STEM looks quite similar to that observed from the same specimen in the normal TEM measurements. FE-STEM measurements have become important for some reasons; for example, suitability for the observations of carbon-based nanomaterials where high beam energy is not always required, since light atom-based material is easily penetrated by less energetic electrons.

3. Typical morphology of "single" gold nanoparticles

Before describing the present results on the morphology of superlattices consisting of monolayer-protected gold nanoparticles, it would be helpful again to refer to the typical shapes of “single” gold nanoparticles. Bulk gold has the fcc structure that is closest-packed. In nanoparticles of gold, there is still debate in the literature regarding the stable structure and external form [27], which arise no doubt from the difficulties in characterizing such small nanomaterials. Several attempts have been made to predict

the structure of gold nanoparticles or clusters using theoretical calculations, yielding shapes of octahedra, cuboctahedra, truncated octahedra, decahedra, and icosahedra [9–11, 27]. The icosahedral or decahedral morphology has fivefold symmetry and is normally non-crystalline. Perfect icosahedral shapes (Mackay icosahedra) are, for example, formed only for magic numbers of atoms, that is, we can obtain the total number of atoms in a k-shell icosahedron as $10/3 \cdot k^3 + 5 \cdot k^2 + 11/3 \cdot k + 1$, giving a discrete sequence of 13, 55, 147, 309, 561, … [28, 29]. Generally, the energies of all these geometries are so similar that they consequently become very hard to differentiate [30–32]. Note that the results of the calculations depend on assumptions regarding the nature of the interatomic interactions [32], how they are modified for surface atoms [31], and use of some empirical parameters [33]. In addition, one should bear in mind that few of any of these small gold nanoparticles or clusters are defect-free and can contain a high density of defects, resulting in the formation of a multiple (fivefold) twinned structure via combinations of low-energy crystal facets in order to reduce their surface energy. This may effectively overcome the internal strain caused by some lattice distortion in the arrangements [11, 34].

4. Materials and methods

Preparation of *N*-acetylglutathione (abbreviated as NAG; the chemical structure is shown in the inset in Fig. 1b), that is, *N*-acetylation of glutathione, was carried out according to the literature procedure [35]. Briefly, glutathione (5.0 g) was dissolved in water (~30 mL) and the solution was added over 1 hr to a mixture of acetic acid/acetic anhydride (50/50 mL) at room temperature. After the addition was complete, the solution was placed on ice and additional acetic anhydride (25 mL) was added. The reaction was allowed to stand overnight while gradually warming to room temperature. A part of the solvent was evaporated, followed by the addition of diethyl ether that causes a precipitation of a crystalline product. The product was then completely washed with diethyl ether.

The synthesis of NAG-protected gold nanoparticles involves preparation of aqueous gold-NAG complex followed by the reduction of the metal ions with sodium borohydride ($NaBH_4$) under a fixed NAG/Au molar ratio. Briefly, 0.5 mmol of $HAuCl_4$ dissolved as 2% (w/v) aqueous solution was first mixed with 1.0 mmol of NAG in 100 mL methanol to give a transparent solution. A freshly prepared ice-cooled 0.2 M aqueous $NaBH_4$ solution (25 mL) was then added at a rate of 2.5 mL per minute under vigorous stirring. The solution turned dark-brown immediately. After further stirring of 1.5 hrs, ethanol/acetic acid (100/1) was added to produce precipitate. The precipitate was washed with the ethanol/acetic acid solution repeatedly through a redispersion–centrifugation process to remove undesirable impurities. Finally, the precipitate dissolved in water was freeze-dried.

We have found that carboxylate-protected gold nanoparticles self-assemble into superlattices or ordered arrays at an air/aqueous solution interface by adding a concentrated hydrochloric acid (HCl) [22–24], so the preparation of 3D nanoparticle superlattices was conducted as follows: The as-prepared NAG-protected gold nanoparticle powder (6.0 mg) was dispersed in 0.05/0.1 M HCl solution (2.0 mL) to form suspensions and stored in a closed vessel for about three weeks. Crystallization or superlattice formation took place at the air/solution interface, showing mirror-like light reflection due to the formation of gold nanoparticle superlattices.

The superlattice samples were scooped on either a Si substrate or a carbon-coated Cu grid, and examined by using an FE-SEM (Hitachi S-4800). FT-IR spectra were measured by using a Horiba FT-210 infrared spectrophotometer using a KBr disk dispersed with the powder sample. The X-ray diffraction measurements were conducted by using Rigaku RINT-2000 with CuKα tube attaching a graphite monochromator.

5. Results and discussion

5.1 Chemical and size characterizations of as-prepared gold nanoparticles

The as-prepared sample analyses reveal the chemical properties of NAG-protected gold nanoparticles. On the basis of FT-IR spectra (Fig. 1a), we obtained the following results on surface chemistry of the nanoparticles: NAG molecules anchor on the gold nanoparticle surface through the sulfur atom in the SH group (as revealed by the disappearance of the S–H stretch mode at ~2570 cm^{-1}). The surface modifier on nanoparticle surfaces contains the bands of amido-I (C=O stretch in NHCO; 1640 cm^{-1}) and amido-II (N–H bending in NHCO; 1540 cm^{-1}) along with those for the stretch modes of COO^- (1600 and 1395 cm^{-1}). The powder X-ray diffraction (XRD) profile shown in Fig. 1b exhibited broad crystalline peaks of gold, and the nanoparticle core diameter, calculated from the Scherrer equation [18], was 1.4 nm using the half width of the intense (111) reflection at $2\theta = 38.2°$. We also conducted TEM measurements for the as-prepared nanoparticle sample; however, the particle size and its distribution could not be estimated because the size was too small to be exactly analyzed.

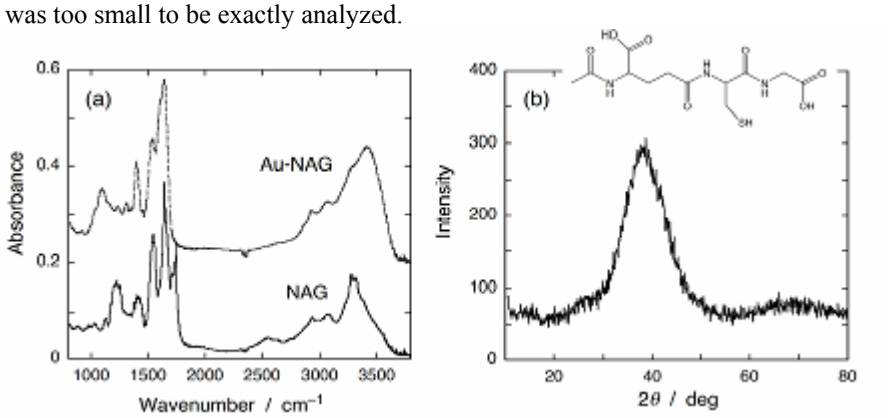

Fig. 1 (a) FT-IR spectra of NAG and NAG-protected gold nanoparticles. (b) XRD profile of the as-prepared NAG-protected gold nanoparticles. The inset shows the chemical structure of NAG (*N*-acetylglutathione).

5.2 Nanoparticle superlattices: Emergence of fivefold symmetry

The NAG-protected gold nanoparticles self-assemble into ordered arrays or superlattices at an air/aqueous solution interface by adding a concentrated hydrochloric acid of 0.05–0.1 M [22–24]. Storage of the solution in a closed vessel for about three weeks provided the superlattices, and their morphology and packing structure were characterized by XRD analyses and FE-SEM observations. The small-angle XRD profile shows several peaks (Fig. 2), suggesting nanometer-scale periodicity caused by the formation of superlattices of NAG-protected gold nanoparticles. The constituent gold nanoparticles were stacked in a pattern of fcc rather than hcp (hexagonal close-packing) with the lattice constant of 11.1 nm (or, center-to-center distance of 7.86 nm) as determined by the simulation of the peak positions. The second-order peak was observed only for 111–reflection, indicating the presence of considerable stacking defects in the superlattices. Note that the lattice constant obtained from the small-angle XRD is larger than that estimated from the average diameter of the as-prepared gold nanoparticles. Actually, the increase in core size of the constituent gold nanoparticles was confirmed by the wide-angle XRD pattern, giving the average diameter of ~6.8 nm (from the Scherrer formula). On the basis of these size estimations, surface-to-surface distance between adjacent nanoparticles in the superlattices is determined to be 1.1–1.5 nm.

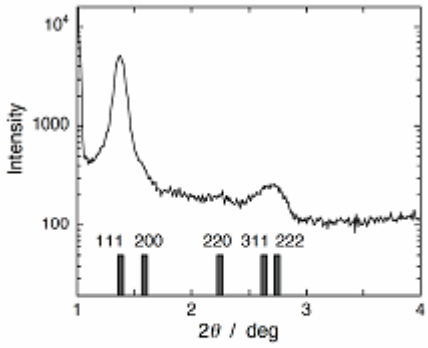

Fig. 2 Small-angle XRD profile of the superlattice sample, suggesting a nanoscale periodicity caused by the formation of ordered arrays of gold nanoparticles.

By comparing this distance with the length of an NAG molecule (~1.0 nm), the surface protecting agents are partly interdigited with each other. Although the mechanism for the size increase is unclear at present, the growth of nanoparticles would take place during the superlattice formation in consideration of the following studies that support our observation: The study on the stability of size-selected glutathione-protected gold nanoclusters shows that some of them were unstable against decomposition whereas thermodynamically stable nanoclusters were enhanced [36]. In addition, the other study on the synthesis of monodisperse nanoparticles indicates that digestive-like ripening, wherein a polydisperse nanoparticles is digested during heating of the solvent, could induce a change of size and its distribution of the monolayer-protected gold particles [37].

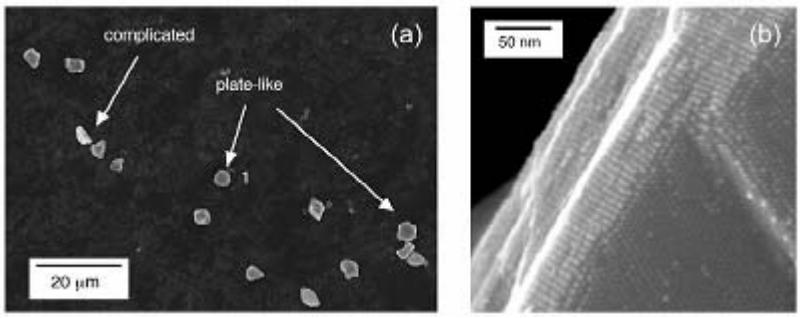

Fig. 3 (a) FE-SEM image of the superlattices of NAG-protected gold nanoparticles on a Si substrate. The superlattices show a variety of morphology having well-defined facets. (b) Magnified image of the superlattice marked with **1**.

FE-SEM observations elucidate a variety of shapes in the 3D nanoparticle superlattices having well-defined or multiple facets, where many of them have plate-like or complicated morphologies (Fig. 3a). Magnified images (Fig. 3b) of the plate-like superlattice marked with **1** clarified the hexagonal close-packed arrangement of nanoparticles with the core size of about 6 nm. In addition, the lattice image observed at the side facets confirmed the 3D ordered arrangement of the nanoparticles. Another example of a superlattice and its magnified surface images are shown in Figs. 4a–4c. In Fig. 4c, a stacking fault (marked with "**SF**") as well as an excellent hexagonal particle arrangement could be observed. Hence it is expected that 3D superlattices of NAG-protected gold nanoparticles can be easily twinned, and the observed complicated morphology having clear facets would result from the twinned structures. In crystallography, the crystal habit depends on the internal structure and the growth conditions, as well as on the kinetics of growth [9]. If the superlattices are formed in thermodynamic equilibrium, their shape

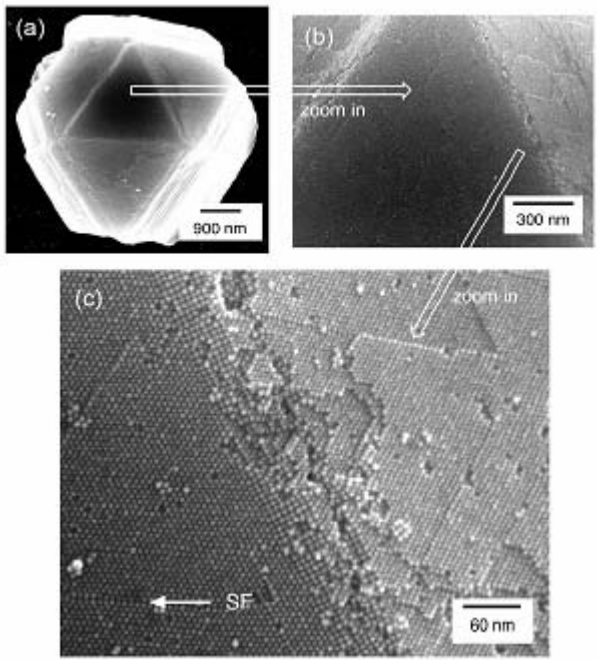

Fig. 4 FE-SEM images of a superlattice of NAG-protected gold nanoparticles. (b) and (c) show the magnified surface images of the superlattice. The image in (c) clarifies the hexagonal close-packed arrangement of nanoparticles and a stacking fault. An example of the stacking fault is marked with "**SF**".

results from minimizing the surface energy. On the contrary, the observed morphologies of the superlattice suggest that its formation is dominated by the kinetics of growth that can promote crystal growth through stacking faults and twins.

We should here also mention that other interesting geometries of the superlattices were found; pentagonal rod, decahedron, and icosahedron as shown in Figs. 5a–5c, respectively. Note that, in Fig. 5b, we cannot see the opposite side of the structure; however, for both symmetry reason and geometrical coincidence of the superlattice with the ideal decahedral model in the same orientation, this geometry should be a decahedron. The strong emphasis is placed on the first observation of fivefold symmetry in the nanoparticle superlattices. These shapes would come from multiple twinning [11]. In the pentagonal rod-like superlattice, the habits were somewhat modified, that is, new faces were developed instead of vertices or edges: Specifically, (i) re-entrant corners (or notches) can be seen. The growth of the notches implies the development of star-shaped superlattices. (ii) The common edges in the structure are truncated to form other faces. Fig. 6 shows the magnified FE-SEM image around the region marked with **2** in Fig. 5a. The triangular face is the close-packed {111}-like plane whereas the truncated face (see the arrow in Fig. 6) shows a tetragonal {112}-like plane. The appeared facets are generally a high-energy surface compared to the close-packed plane due to high-index crystallography planes, but the edge truncation is very effective for lowering the surface/volume ratio.

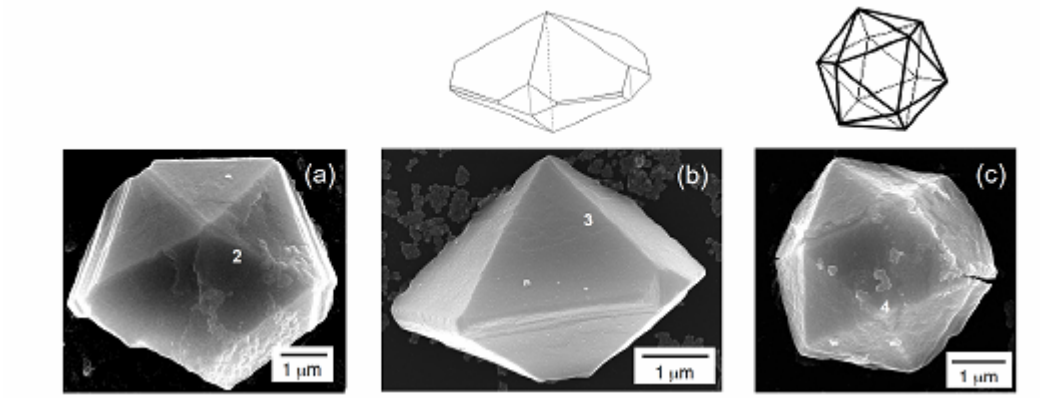

Fig. 5 Superlattices of (a) pentagonal rod-like, (b) decahedral, and (c) icosahedral shapes. The sketches on the upper row show the geometrical model of Marks decahedron having re-entrant corners (for (b)) and that of icosahedron (for (c)) in the same orientations.

It is known that the two most typical fivefold twinning are decahedron and icosahedron. A decahedron is assembled from 5 tetrahedral subunits sharing an edge. An icosahedron is assembled using 20 tetrahedral subunits via sharing an apex [11]. Intrinsically, tetrahedral subunits in fcc cannot form a complete space-filling structure, so that there remains angular misfit yielding internal strain. The strain is relaxed by a reduction of surface energy up to a certain size above which transformation to single crystalline particles is expected. Hence a fivefold twined particle is commonly bounded by the lowest-energy triangular facets. In regular decahedra, they have a large surface/volume ratio, which can be lowered by truncating the edges around the common basis, thus obtaining the Ino decahedra with five {100}-like facets [38]. An even better structure is the

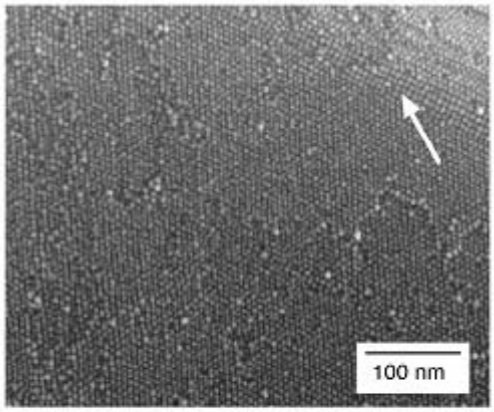

Fig. 6 Magnified FE-SEM image at the vicinity of the edge region marked with **2** in Fig. 5a. The arrow indicates the truncated common edge.

Marks decahedra, obtained by introducing re-entrances that separate the {100}-like facets [34]. In Fig. 5b, the observed re-entrant corners are well characterized by a typical Marks decahedron whose schematic drawing is shown at the upper row of the image.
On the other hand, an icosahedral particle normally contains a larger strain inside due to the distortion of the intershell and intrashell distances, so that this form could be present only at small sizes in single metal nanoparticles. For example, the size limit of 27.35 nm has been obtained in icosahedral silver nanoparticles, whereas that of 273.3 nm in decahedra [38–40]. Note that the total number of silver atoms in an icosahedral nanoparticle of ~27 nm can be approximately estimated to be $4–5 \times 10^5$, corresponding to 40–50 shells [41]. Surprisingly, in Fig. 5c, $1–2 \times 10^8$ nanoparticles are included in the superlattice of ~4 μm assuming that they are made of spheres of 7.9 nm in diameter (= center-to-center distance between adjacent nanoparticles), which correspond to 300–400 shells (For the estimation, a Mackay icosahedron is assumed.) [28, 41]. This is probably due to the fact that a large relaxation of the internal strain caused by the size non-uniformity (or flexibility) of the constituent nanoparticles makes the icosahedral structure much stable. However, the strain remained in the structure could collapse the regular shape when handling the superlattice samples distributed at the air/solution interface (see one edge in Fig. 5c).

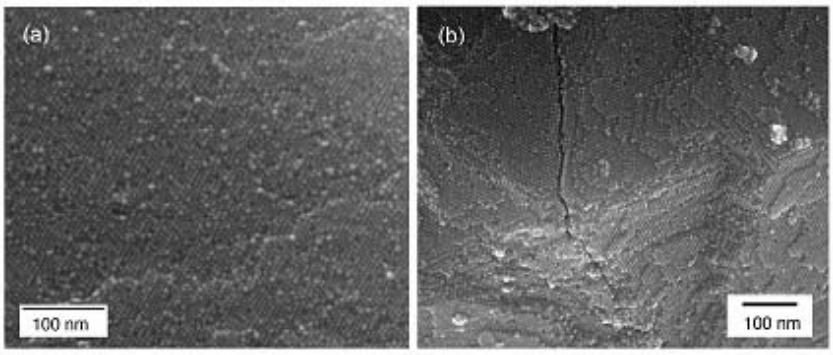

Fig. 7 (a) Magnified surface image around the region marked with **3** in Fig. 5b. (b) Magnified surface image around the regions marked with **4** in Fig. 5c. The nanoparticle arrangement in the region of **3** differs from that of **2** or **4** of {111}-like planes.

High-resolution FE-SEM images at the boundary surfaces of decahedral and icosahedral superlattices provide interesting characteristics on the arrangements of nanoparticles. Figs. 7a and 7b show the magnified surface images around the regions marked with **3** and **4** in Fig. 5, respectively. For example, a face referred to as **4** is in the close-packed hexagonal arrangement of nanoparticles ({111}-like planes), whereas that referred to as **3** are in distorted tetragonal (non-close-packed) arrangements that are ascribed to different index planes. The results indicate that these surface planes having different packing structures are energetically similar to each other. Since the individual NAG-protected gold nanoparticles are composed of both nanoscaled metallic-core and the molecular-shell parts, multiple interactions among the nanoparticle units that involve van der Waals and hydrogen bonding interactions would contribute to this intriguing phenomenon.

4. Conclusion

In conclusion, 3D gold nanoparticle superlattices were produced at an air/solution interface under highly acidic conditions. The surface of the gold nanoparticles used was protected by *N*-acetylglutathione (NAG) that can bind the constituent nanoparticles via hydrogen bonds. Morphological studies by FE-SEM revealed that the superlattices formed fivefold symmetric structures such as pentagonal rod, decahedron, and icosahedron, which were probably developed by multiple twinning. High-resolution surface images of the superlattices in fivefold symmetry showed excellent ordered arrangements of

nanoparticles with both close-packed and non-close-packed structures. The field of fivefold twinned structures is a very broad and complicated one ranging from cluster science to surface science, so that we believe that our findings will give a new development of this fascinating subject in nanoscience.

Acknowledgements The authors thank Mrs. Takayuki Minami and Akihiko Hori for their collaboration. The present work was financially supported by Grant-in-Aids for Scientific Research from MEXT (B: 19310076 (H. Y.) and S: 16101003 (K. K.)).

References

[1] B. L. Cushing, V. L. Kolesnichenko and C. J. O'Connor, Chem. Rev. **104**, 3893 (2004).
[2] M-C. Daniel and D. Astruc, Chem. Rev. **104**, 293 (2004).
[3] R. L. Whetten, M. N. Shafigullin, J. T. Koury, T. G. Schaaff, I. Vezmar, M. M. Alvarez and A. Wilkinson, Acc. Chem. Res. **32**, 397 (1999).
[4] M. Brust, M. Walker, D. Bethell, D. J. Schiffrin and R. J. Whyman, Chem. Soc. Chem. Commun. 801 (1994).
[5] A. C. Templeton, W. P. Wuelfing and R. W. Murray, Acc. Chem. Res. **33**, 27 (2000).
[6] B. Wiley, Y. Sun, B. Mayers and Y. Xia, Chem. Eur. J. **11**, 454 (2005).
[7] I. O. Sosa, C. Noguez and R. G. Barrera, J. Phys. Chem. B **107**, 6269 (2003).
[8] C. J. Murphy and N. R. Jana, Adv. Mater. **14**, 80 (2002).
[9] Z. L. Wang, J. Phys. Chem. B **104**, 1153 (2000).
[10] L. D. Marks, Rep. Prog. Phys. **57**, 603 (1994).
[11] H. Hofmeister, in: *Encyclopedia of Nanoscience and Nanotechnology*, edited by H. S. Nalwa, Vol. 3 (American Scientific, Stevenson Ranch, 2004), 431.
[12] H. Yao, S. Sato and K. Kimura, in: *Nanoparticle Assemblies and Superstructures,* edited by N. A. Kotov (Taylor & Francis, Boca Raton, 2006), 601.
[13] M. Brust and C. J. Kiely, Colloids Surf. A **202**, 175 (2002).
[14] J. F. Sampaio, K. C. Beverly and J. R. Heath, J. Phys. Chem. B **105**, 8797 (2001).
[15] C. J. Zhong and M. M. Maye, Adv. Mater. **13**, 1507 (2001).
[16] J. J. Storhoff and C. A. Mirkin, Chem. Rev. **99**, 1849 (1999).
[17] M. Burghard, G. Philipp, S. Roth, S. K. von Klitzing, R. Pugin and G. Schmid, Adv. Mater. **10**, 842 (1998).
[18] S. Chen and K. Kimura, Langmuir **15**, 1075 (1999).
[19] H. Yao, O. Momozawa, T. Hamatani and K. Kimura, Chem. Mater. **13**, 4692 (2001).
[20] H. Yao, O. Momozawa, T. Hamatani and K. Kimura, Bull. Chem. Soc. Jpn. **73**, 2675 (2000).
[21] G. A. Jeffrey, *An Introduction to Hydrogen Bonding* (Oxford University Press, Oxford, 1997).
[22] K. Kimura, S. Sato and H. Yao, Chem. Lett. 372 (2001).
[23] S. Sato, H. Yao and K. Kimura, Physica E **17**, 521 (2003).
[24] H. Yao, H. Kojima, S. Sato and K. Kimura, Langmuir **20**, 10317 (2004).
[25] J. Pawley, Scanning **19**, 324 (1997).
[26] K. L. Bunker, J. C. Gonzalez, D. A. Batchelor, T. J. Stark, and P. E. Russell, *Science, Technology and Education of Microscopy: an Overview*, edited by A. Méndez-Vilas, Vol. 1 (FORMATEX, Badajoz, Spain 2002).
[27] C. L. Cleveland, U. Landman, T. G. Schaaf and M. N. Shafigullin, Phys. Rev. Lett. **79**, 1873 (1997).
[28] A.L. Mackay, Acta Cryst. **15**, 916 (1962).
[29] W. Eberhardt, Surf. Sci. **500**, 242 (2002).
[30] T. X. Li, S. Y. Yin, Y. L. Ji, B. L. Wang, G. H. Wang and J. J. Zhao, Phys. Lett. A **267**, 403 (2000).
[31] J. M. Soler, I. L. Garzón and J. D. Joannopoulis, Solid State Commun. **117**, 621 (2001).
[32] I. L. Garzón, K. Michaelian, M. R. Beltrán, A. Posada-Amarillas, P. Ordejón, E. Artacho, D. Sánchez-Portal and J. M. Soler, Phys. Rev. Lett. **81**, 1600 (1998).
[33] H. B. Liu, J. A. Ascencio, M. Perez-Alvarez and M. J. Yacaman, Surf. Sci. **491**, 88 (2001).
[34] L. R. Wallenberg, J. O. Bovin and G. Schmid, Surf. Sci. **156**, 256 (1985).
[35] E. J. Levy, M. E. Anderson and A. Meister, Anal. Biochem. **214**, 135 (1993).
[36] Y. Negishi, K. Nobusada and T. Tsukuda, J. Am. Chem. Soc. **127**, 5261 (2005).
[37] B. L. V. Prasad, S. I. Stoeva, C. M. Sorensen and K. J. Klabunde, Langmuir **18**, 7515 (2002).
[38] S. Ino, J. Phys. Soc. Jpn. **27**, 941 (1969).
[39] F. Silly and M. R. Castell, Appl. Phys. Lett. **87**, 213107 (2005).
[40] F. Baletto and R. Ferrando, Rev. Mod. Phys. **77**, 371 (2005).
[41] S. C. Hendy and J. P. K. Doye, Phys. Rev. B **66**, 235402 (2002).